Global simulations of multi-frequency HF signal absorption for direct observation of middle atmosphere temperature and composition

Alireza Mahmoudian[1], Michael J Kosch[2,3,4], Reza Mohammadi Baghaei[1]

[1]Institute of Geophysics, University of Tehran, Iran.
[2]Department of Physics, Lancaster University, Lancaster, UK.
[3]South African National Space Agency (SANSA), Hermanus, South Africa
[4]Dept. of Physics and Astronomy, University of the Western Cape, Bellville, South Africa

Key Points:

- First study on a new concept of a multi-frequency HF beacon for the direct measurement of D-region absorption is presented.
- Full physics-based model of HF radio absorption in the upper atmosphere is developed.
- A machine learning model is developed and the capability of the model in estimation of D and E-region constituents is examined.

Corresponding author: Dr. Alireza Mahmoudian, `a.mahmoudian@ut.ac.ir`

Abstract

This paper presents the first numerical study on a new concept for the direct measurement of D-region absorption in the HF band. Numerical simulations based on the Appleton–Hartree and Garrett equations of refractive index are presented. Electron temperature as a result of HF radio pumping of the ionosphere is included in the calculations using proper numerical formulation. Both O- and X-mode polarizations are taken into consideration. A global map of HF absorption in the northern hemisphere is calculated. Detailed calculations of HF radio wave absorption as it propagates through the lower atmosphere are presented. The effect of several parameters on the amount of absorption is calculated. The best frequencies to be used for the purpose of this study are discussed. A machine learning model is developed and the capability of the model in estimation of D and E-region constituents includes N_2, O, O_2, as well as T and N_e is examined. Such a technique can also lead to global mapping of HF absorption and improve OTHR (over-the-horizon-radar) performance.

1 Introduction

The lower atmosphere has a great impact on the propagation of high-frequency radio waves. These effects could result in the distortion of HF signal and may limit the applications of this frequency band specifically for remote sensing applications. Remote sensing of the ionosphere and ionospheric tomography has been an area of great interest among space physicists. The satellite-based ionospheric tomography using flying beacons as well as satellite radio signal transmission and ground reception has been studied over the past several decades. There are ground-based instruments such as riometers, radio receivers that continuously monitor the power received from extraterrestrial radio sources (Little and Leinbach, 1959), which are designed to measure D-region absorption. While using a higher operating frequency for riometers (VHF band) may reduce the sensitivity to the absorption, these signals must pass through the ionosphere, they are subject to varying attenuation due to changes in the electron density.

The first use of beacons on rockets for measuring ionospheric parameters was carried out by Seddon (1953). The first mission had the continuous wave (CW) radio transmissions from the rocket at HF frequencies (4.27 MHz or 7.75 MHz and their 6th harmonic). Further details on ionospheric layer profiling using rocket beacon signals are described by Jackson (1954), Friedman (1959), Maeda (1970), Evans (1977), Smith and Gilchrist (1984), and Bernhardt et al. (1993).

The Naval Research Laboratory (NRL) has developed a Coherent Electromagnetic Radio Tomography (CERTO) beacon with available frequencies of VHF (150 MHz) and UHF (400 MHz) in collaboration with the Air Force Research Laboratory (AFRL). The developed CETRO beacon has been used on Communications/Navigation Outage Forecast System (C/NOFS) satellite (de La Beaujardie‘re et al., 2004) to register low-latitude scintillations recorded by the AFRL Scintillation Decision Aid (SCINDA) network of ground receivers (Groves et al., 1997; Caton et al., 2004; Bernhardt et al., 1998). Bernhardt et al. (1993) and Bernhardt and Huba (1993) developed numerical simulations, known as computerized ionospheric tomography (CIT), which can build the reconstructive imaging of F-region irregularities.

The heating of the ionospheric plasma by modulated high-frequency waves leads to physical processes with a wide range of scales due to elevated T_e/T_i (electron to ion temperature). Artificial modulation of D-region plasma to diagnose dusty plasma region associated with polar mesospheric summer echoes had been an area of research over the past two decades (Havnes, 2004; Scales, 2004; Scales and Mahmoudian 2016; Mahmoudian et al., 2020). The polar mesospheric summer echoes (PMSE) are strong radar echoes associated with polar mesospheric clouds (PMC), which are natural ice/dust layers in the polar region in the altitude range of 80 to 90 km and are widely believed to be a direct manifestation of global warming. A remote sensing technique has been developed to study this region during radio modulation by high-power radio waves and multi-frequency radar observations. Our recent work has shown that the modified ionospheric condition due to radio wave heating of the ionosphere can lead to the enhanced absorption of the radio waves in the ionosphere. The estimated D-region absorption at 8 MHz has been studied to measure the PMSE (Senior et al., 2011; 2016).

The idea of implementing a multi-frequency radio beacon in low Earth orbit (LEO) has been used for many years to study ionospheric irregularities through the scintillation information of the passing signal through the ionosphere using GPS signals. The present work describes the general idea of developing a multi-frequency HF beacon to be used for measuring ionospheric and upper atmosphere parameters. The basic idea is to develop the first multi-frequency high-frequency (HF) beacon to fly on a CubeSat in order to obtain the first direct measurement of D-region parameters. Other applications of Iran's first CubeSat mission with multi-frequency HF beacon, REEIMA: Radio Explorer for Earth, Ionosphere, Mesosphere, and Atmosphere, to measure ionospheric, mesospheric, and atmospheric parameters are introduced. Specifically, the frequency selection for the HF beacon by including a detailed computational model of HF absorption in the D-region is considered. The absorption model is capable of calculating the loss rate associated with vibrational and rotational cooling of electrons due to the presence of neutral atoms. The ionospheric model including the Appleton-Hartree and Garrett equations of refractive index are considered. The model is also designed to calculate the absorption and enhanced electron temperature in the presence of modulated mesospheric conditions by high-power HF radio waves. A machine learning model is developed and the capability of the model in estimation of D and E-region constituents includes N_2, O, O_2, as well as T and N_e is introduced. The discussion on remote sensing of mesospheric parameters based on the simulation results is provided.

2 Computational Model

The model used in this study includes a general expression of electron temperature enhancement in the presence of transmitted HF radio wave from the ground. This expression can be written as follow which includes the time variation of electron temperature

$$\frac{3}{2}k_B N_e \frac{dT_e}{dt} = -2S(t)\frac{\omega}{c}Im\mu(N_e, T_e) - N_e L(T_e, T_n) \tag{1}$$

where k_B is Boltzmann's constant, N_e, T_e are the electron number density and temperature, w is the disturbing wave angular frequency, c is the free space speed of light, m is the complex refractive index of the disturbing wave and $L(T_e, T_n)$ is the electron energy loss function where T_n is the neutral gas temperature. O_2, N_2, and O neutral gases are considered in this work. The first term on the right represents the energy gained by electrons due to the absorption of the disturbing wave. This equation includes the time varying power flux $S(t)$, which modifies the background electron temperature at the interaction region. The model is set up such that the ordinary Appleton–Hartree formula and generalized refractive index of Garrett (1985) can be implemented in the calculations. One of the main features that make this model distinct in comparison with other time dependent heating models is the inclusion of self-absorption of high-power HF heating wave. One of the practical ways to measure the absorption coefficient is to send a low power HF pulse and high-power HF heating wave in an alternative sequences. The high-power HF pulse modifies the background electron density and temperature in the D-region and enhances the absorption coefficient. Therefore, such experimental set up can be used to measure the natural absorption in the absence of heating signal as well as in the modified background mesospheric conditions.

2.1 Refractive Index

The electromagnetic wave propagation in different materials and environment is mostly governed by refractive index of the region. The Appleton–Hartree equation of refractive index, which can be written in the following form, can describe the propagation of electromagnetic waves in the cold and magnetized plasma:

$$\mu^2 = 1 - \frac{X}{1 - Iz\frac{\frac{1}{2}Y^2\sin^2\theta}{1-X-iZ} \pm \frac{1}{1-X-iZ}\left(\frac{1}{4}Y^4\sin^4\theta + Y^2\cos^2\theta(1-X-iZ)\right)} \tag{2}$$

where $X = (\omega_0^2)/\omega^2, Y = \omega_{ce}/\omega, Z = \nu/\omega, \omega$ denotes the frequency of the propagation signal, ω_0 is the electron plasma frequency, Ω_{ce} is the electron gyro-frequency, θ represents the angle between the ambient magnetic field vector and the wave vector, and ν is the electron neutral collision frequency. It should be noted that these parameters vary with altitude. As can be seen from this expression, the radio wave propagation in the ionosphere and the presence of cold magnetized plasma will depend on the direction of propagation concerning the background magnetic field, transmission frequency as well as background ionospheric parameters. It should be noted that the generalized refractive index of Garrett (1985, 1991) has also been implemented in the model. It has been shown that the difference between Appleton–Hartree and Garrett's refractive index is less than ~ 0.1 and 0.03 dB/km for the frequency range 8-16 MHz and larger than 16 MHz, respectively. A comparison of the results obtained using the two models is provided in the following sections.

2.2 Cooling model

Studying the electron temperature variation in the ionosphere requires a good insight to the possible heating, cooling, energy flow processes in the natural or artificially modified conditions. The enhanced electron temperature as a result of external HF pump heating could be reduced due to the cooling of electrons by neutral particles present in this region. The cooling process is mainly due to the vibration or rotational collision of electrons with neutral particles. The cooling efficiency varies significantly with the type of neutral atoms. Considering the major neutral particles of N_2, O_2 and O in this region, the associated densities and temperature are imported from NRLMSISE-00 model. The main neutral atoms and cooling processes used in this study are the vibrational and rotational cooling of electrons by N_2 and O_2 atoms.

The cooling rate (loss rate) for the N_2 atom and due to rotational excitation can be written in this form (Schunk and Nagy, 1978) (SN78)

$$L = 2.9e \times 10^{-20} N_e \times N_2(T_e - T_n)/\sqrt{T_e} \tag{3}$$

where L is the loss rate, n_e is the electron density, N_2 is the density of Nitrogen atoms, T_n is the neutral temperature, T_e is the electron temperature. The cooling rates for O_2 atom using Pavlov's expression can be written as follow (Pavlov, 1998a,b,c).

$$L = 6.9e \times 10^{-20} N_e \times O_2(T_e - T_n)/\sqrt{T_e} \tag{4}$$

According to Pavlov, 1998c, the N_2 rotational excitation is similar to SN78 with a correction factor of 1.255, which is considered in this study. It should be noted that cooling rates based on Pavlov (1998a,b,c) are refereed to P98 formulation in the text. The vibrational cooling by N_2 atom can be written in the following form using the SN78 formula

$$f = 1.06 \times 10^4 + 7.51 \times 10^3 \times tanh(1.10 \times 10^{-3}(T_e - 1800)) \quad (5)$$

$$g = 3300 + 1.233 \times (T_e - 1000) - 2.056 \times 10^{-4} \times (T_e - 1000)(T_e - 4000) \quad (6)$$

$$L = 2.99e \times 10^{-18} N_e N_2 \times e^{(\frac{f(T_e-2000)}{(2000T_e})}(1 - e^{(-\frac{g(T_e-T_n)}{(T_eT_n)}}) \quad (7)$$

The vibrational cooling by N_2 atom using P98 formulation can be written in the following form

$$L = N_e N_2[(1 - e^{-3353/T_{vib}}) \times \sum_{v=1}^{10} Q_{0v}(1 - e^{[v3353(T_e^{-1} - T_{vib}^{-1})]}) +$$

$$(1\text{-}e^{-3353/T_{vib}})e^{-3353/T_{vib}} \times \textstyle\sum_{v=2}^{9} Q_{1v}(1 - e^{[(v-1)3353(T_e^{-1} - T_{vib}^{-1})]})](8)$$

where T_{vib} is assumed to be equal to T_n. The Q_{0v} and Q_{1v} (the electron energy transfer rates) are calculated for $T_e > 1500$ and $T_e \leq 1500$, respectively, and based on coefficients provided in Table 2 and 3 in Pavlov (1998a).

The vibrational cooling by O_2 atom can be written in the following form Schunk and Nagy, (1978) (SN78)

$$h = 3300 - 839 \times sin(1.91 \times 10^{-4} \times (T_e - 2700)) \quad (9)$$

$$L = 5.19e \times 10^{-19} N_e O_2 \times e^{(\frac{h(T_e-700)}{(700T_e)}} \left(1 - e^{\frac{-2770(T_e-T_n)}{(T_eT_n))}}\right) \quad (10)$$

The O_2 rotational excitation from SN78 is provided in implemented using the expression below

$$L = 5e \times 6.9 \times 10^{-20} \times (N_e O_2(T_e - T_n))/\sqrt{T_e} \quad (11)$$

O_2 rotational excitation and cooling rate from Pavlov (1998a) (P98) can be written in the following form:

$$L = 5.2e \times 10^{-21} \times \frac{N_e O_2(T_e - T_n)}{\sqrt{T_e}} \quad (12)$$

O_2 vibrational excitation using formula based on expressions 1-5 and Table 1 in Jones et al. (2003) (J03). The calculation of N_2 vibrational excitation from Campbell et al. (2004) is also considered.

Three scenarios are considered for the combination of the cooling rates shown in expressions (3-12). In the standard scenario, N_2 vibrational and rotational excitation

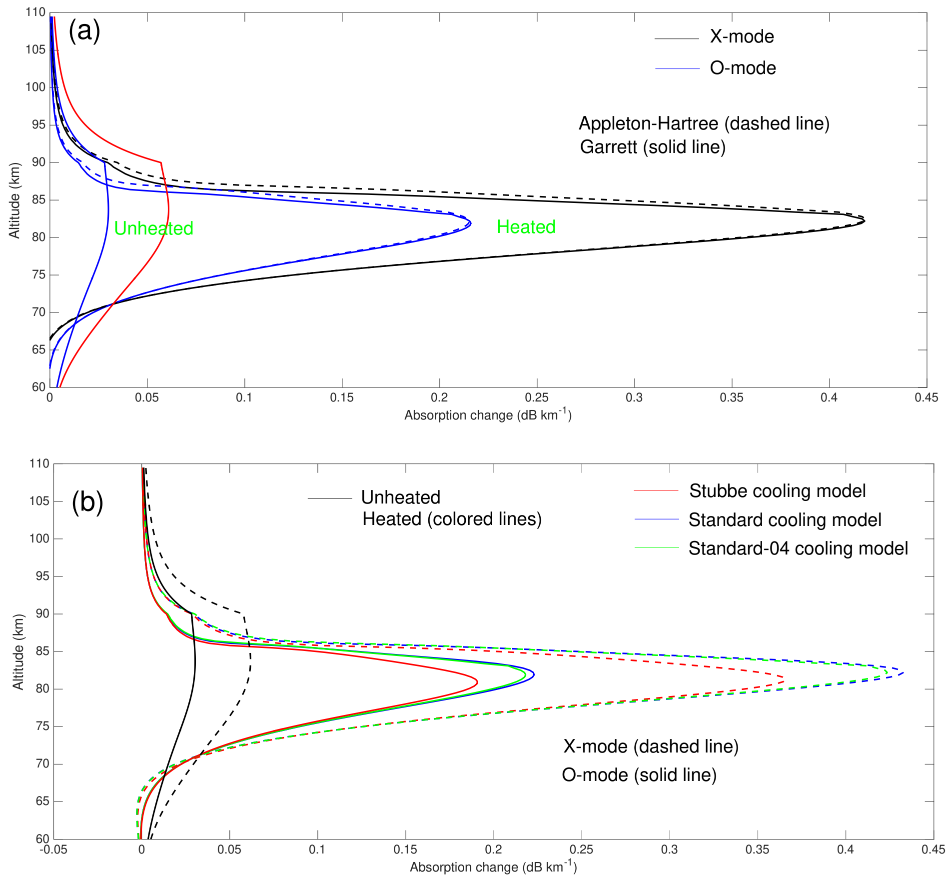

Figure 1. a) O-mode and X-mode absorption versus altitude obtained using Appleton-Hartree formula for the refractive index assuming phase propagation parallel to the magnetic field and Garrett's generalized refractive index formula in the heated and unheated D-region. b)The effect of different cooling models on the calculated absorption amplitude in a) unheated and b) heated ionospheric condition. The transmission frequency of 8 MHz is considered.

and N_2 rotational cooling using P98 formulation and O_2 vibrational excitation using J03 formula is used. The Standard-04 cooling model based on N_2 and O_2 rotational excitation using P98 model, O_2 vibrational excitation using J03 formula, and N_2 vibrational cooling using C04 is implemented. The Subbe cooling model based on N_2 and O_2 rotational and vibrational excitation obtained using SN78 is used. A close comparison of three scenarios on the associated estimated HF absorption will be examined in the following sections. As discussed, the main concept to investigate in section 2 is to evaluate available theories for cooling models to explore its impact on the absorption calculation versus altitude and at different transmission frequencies. This is a critical step to show that model is robust for different estimations included in the cooling rates formulations. As it will be shown later in the paper, the degree of variation in the absorption results based on the three cooling models proposed in this paper is negligible.

3 Numerical Results

The numerical solution to the expression of electron temperature variation is considered to calculate the electron temperature enhancement during radio wave heating

Cooling approach	Standard	Standard 04	Stubbe
Cooling rates	N_2 Vibrational P98 N_2 Rotational P98 O_2 Vibrational J03 O_2 Rotational P98	N_2 Vibrational C04 N_2 Rotational P98 O_2 Vibrational J03 O_2 Rotational P98	N_2 Vibrational SN78 N_2 Rotational SN78 O_2 Vibrational SN78 O_2 Rotational SN78

Table 1:The cooling rates used in this study based on the combination of rates for vibrational and rotational N_2 and O_2 using SN78 (Schunk and Nagy, 1978), P98 (Pavlov, 1998a), J03 (Jones et al., 2003) and C04 (Campbell et al., 2004) calculations.

of the ionosphere as well as the modified electron-neutral collision frequency. The amount of signal absorption as a function of electron temperature can be obtained from

$$S_{out}(t) = \left(\frac{z}{z+\Delta z}\right)^2 S(t) + 2S(t)\Delta z \frac{\omega}{c} Im\mu(N_e, T_e) \tag{13}$$

In this approach the region of interest can be divided to small sections with a thickness of Δz. The input power is S(t) and the output power at the end of each section and including the absorbed signal is shown by $S_{out}(t)$. The value of output power at each altitude is calculated with a delay to include the absorption in the lower layers.

Several parameters are used in this study such as the polarization of the transmitted signal (O- and X-mode) and for transmission frequency in the range of 2 MHz to 30 MHz in the natural and artificially modified ionospheric conditions. The main goal of this study is to determine the characteristics of the HF signal within the HF band to develop a remote sensing technique to measure absorption in the D-region. This approach and the selected frequencies will be used to design the future CubeSat mission (REEIMA: Radio Explorer for Earth, Ionosphere, Mesosphere, and Atmosphere). The main idea is to design a multi-frequency HF beacon to fly on first Iran's CubeSat and to measure ionospheric, mesospheric, and atmospheric parameters. The basic changes of passing the signal through the ionosphere including absorption, scattering, diffraction, amplitude and phase scintillation, Faraday rotation, spectral Doppler shift will be used to determine the basic parameters of the ionosphere and mesosphere. The described REEIMA CubeSat mission is designed to be used for other applications such as gravity wave characterization. The review of the mission and applications are beyond the scope of the current paper and will be discussed in more detail in the following papers.

Figure 1 presents the comparison of the HF absorption profile at 8 MHz for results obtained using Garrett and AH refractive indices. Figures 1a and b present the absorption profile in the unheated and heated (elevated T_e/T_i) conditions. Blue and black lines present the O- and X-mode results. The main difference between the results obtained using Garrett and AH formula of refractive index appears near the maximum amplitude. The difference in predicted values of total absorption is similar for both ionospheric conditions (and at each transmission frequency). Total HF absorption associated with the results presented in Figure 1, is provided in Table 2. According to Table 2, the difference between the estimated total absorption is of the order of 0.032 dB (0.07 dB) for the O-mode (X-mode) in the unheated condition. The difference between the estimated total absorption of 0.24 dB (0.42 dB) for the O-mode (X-mode) in the heated condition is predicted. The results show that the refractive index model used in the calculations has a minimum effect on the technique proposed in this paper. Moreover, implementing HF absorption measurements at multi-frequency in heated and unheated conditions (within a short period to have a similar ionospheric condition) would result in the calibration of the instrument and accurate determination of ionospheric constituents.

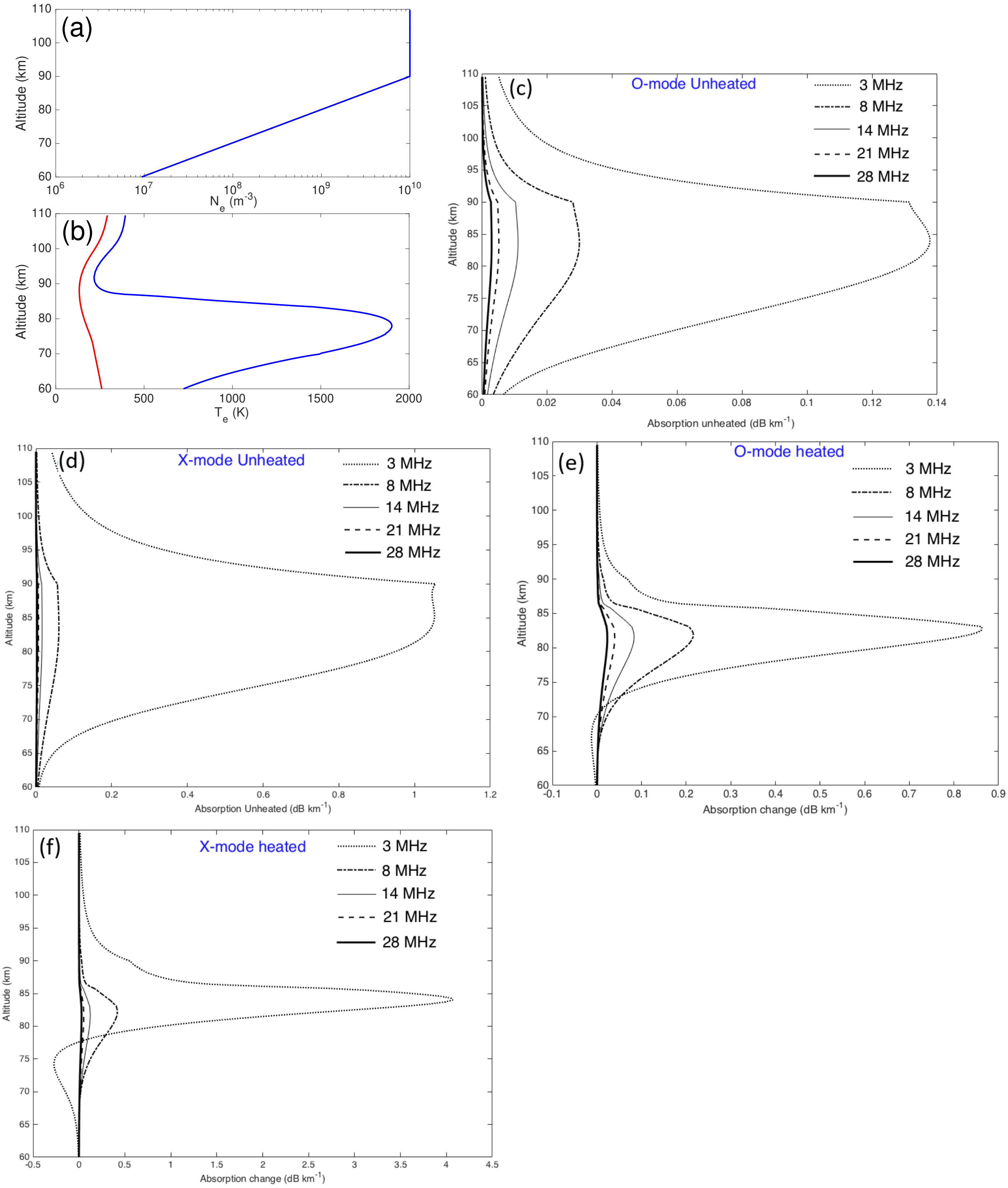

Figure 2. a) Typical background electron density profile, b) electron temperature profile c, d) Absorption for the unheated mesospheric condition and differential absorption (dB km^{-1}) with respect to the heated ionosphere for transmission frequencies (f_0) of 2, 8, 16, 24, 28 MHz for O-mode and X-mode, e, f) Similar to c,d for X-mode.

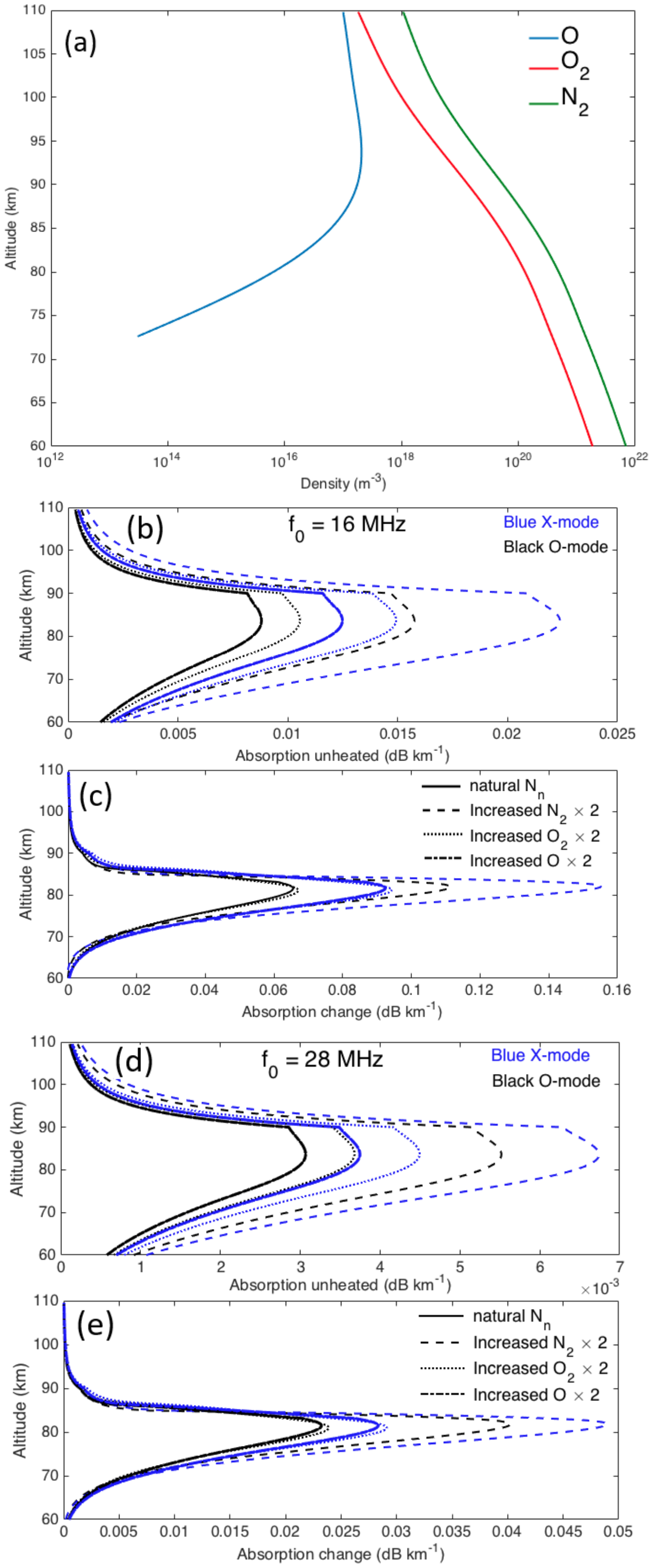

Figure 3. a) Background neutral densities derived from MSIS model b,c) The variation of the absorption at 16 MHz and d,e) 28 MHz with varying neutral densities of N_2, O_2, O. The unheated ionospheric plasma conditions are shown in panels b and d. Panels c and e represent the results corresponding to artificially heated ionospheric plasma.

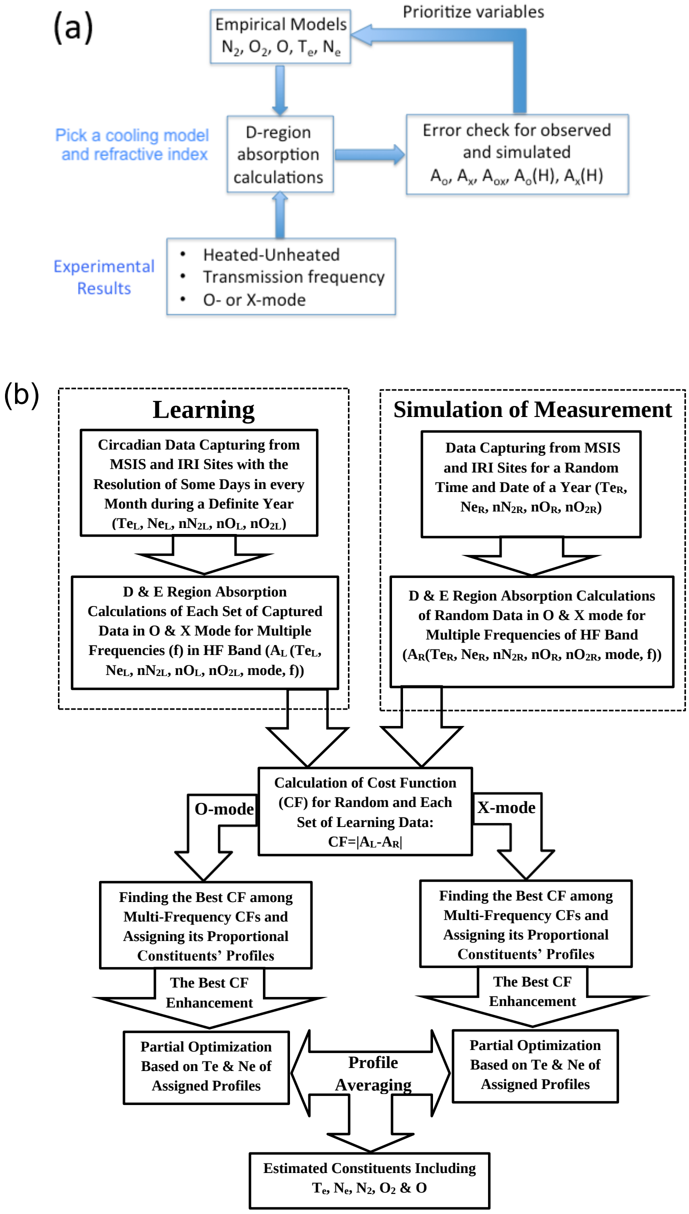

Figure 4. a) Data assimilation diagram b) developed machine learning (ML) procedure

	Absorption O-mode	Absorption X-mode	Phase O-mode	Phase X-mode
Garrett's generalized refractive index formula				
Unheated	0.422	0.825	4173.755	4173.267
Heated	2.175	3.816	4173.861	4173.501
Appleton-Hartree formula for the refractive index				
Unheated	0.454	0.894	4173.753	4173.264
Heated	2.421	4.238	4173.871	4173.529

Table 2: Total HF absorption associated with the results presented in Figure 1. The calculations are made using Garrett and AH formula of refractive index. Unheated and artificially modulated ionosphere using HF radio waves are considered.

	Absorption O-mode	Absorption X-mode	Phase O-mode	Phase X-mode
3 MHz				
Unheated	1.917	11.582	1563.127	1559.207
Heated	7.609	24.044	1563.744	1562.733
8 MHz				
Unheated	0.454	0.894	4173.753	4173.264
Heated	2.421	4.238	4173.871	4173.529
14 MHz				
Unheated	0.173	0.256	7305.399	7305.241
Heated	1.034	1.474	7305.434	7305.298
21 MHz				
Unheated	0.082	0.107	10958.680	10958.610
Heated	0.519	0.666	10958.693	10958.628
28 MHz				
Unheated	0.048	0.059	14611.855	14611.816
Heated	0.310	0.375	14611.861	14611.824

Table 3:Total absorption and phase variation of the passing HF signal through the natural and artificially modified mesospheric condition by high-power HF heating wave for the O- and X-mode signals at f_0 = 2, 8, 16, 24, and 28 MHz.

Detailed investigation of cooling rate models presented in Table 1, is provided in Figure 2. O-mode and X-mode absorption versus altitude obtained using Appleton-Hartree formula for the refractive index assuming phase propagation parallel to the magnetic field and Garrett's generalized refractive index formula in the heated and unheated D-region. The transmission frequency of 8 MHz is considered. Three cooling models associated with N_2 and O_2 vibrational and rotational cooling are used. The calculated HF absorption profile associated with Stubbe, Standard, and Standard-04 cooling models are presented in green, blue, and black colors, respectively. According to Figure 2a, no change in HF absorption profile is seen for different cooling models used in this paper. Both O- and X-mode absorption profiles at 8 MHz are consistent with various cooling rates included. In heated plasma conditions, the HF absorption profiles show a small discrepancy as shown in Figure 2b. The difference between the predicted absorption profile using Standard and Standard-04 cooling models is negligible for both O- and X-modes. Considering the possibility of conducting HF absorption measurement in a short amount of time (to probe the region of D- and E-regions) in heated and unheated ionospheric conditions, the best model to fit the observations can be determined.

Typical:

8 MHz			
ΔA_O(H-UH)	ΔA_X(H-UH)	ΔA_{OX}(UH)	ΔA_{OX}(H)
1.74	2.691	0.403	1.624
16 MHz			
ΔA_O(H-UH)	ΔA_X(H-UH)	ΔA_{OX}(UH)	ΔA_{OX}(H)
0.619	0.841	0.052	0.274
24 MHz			
ΔA_O(H-UH)	ΔA_X(H-UH)	ΔA_{OX}(UH)	ΔA_{OX}(H)
0.311	0.386	0.015	0.09

N2*2

8 MHz			
ΔA_O(H-UH)	ΔA_X(H-UH)	ΔA_{OX}(UH)	ΔA_{OX}(H)
2.116	3.281	0.672	1.837
16 MHz			
ΔA_O(H-UH)	ΔA_X(H-UH)	ΔA_{OX}(UH)	ΔA_{OX}(H)
0.964	1.281	0.097	0.414
24 MHz			
ΔA_O(H-UH)	ΔA_X(H-UH)	ΔA_{OX}(UH)	ΔA_{OX}(H)
0.441	0.541	0.028	0.128

Ne*2

8 MHz			
ΔA_O(H-UH)	ΔA_X(H-UH)	ΔA_{OX}(UH)	ΔA_{OX}(H)
2.498	4.026	0.882	2.183
16 MHz			
ΔA_O(H-UH)	ΔA_X(H-UH)	ΔA_{OX}(UH)	ΔA_{OX}(H)
0.932	1.256	0.112	0.436
24 MHz			
ΔA_O(H-UH)	ΔA_X(H-UH)	ΔA_{OX}(UH)	ΔA_{OX}(H)
0.425	0.523	0.032	0.13

Table 4:Detailed study of electron density N_e and N_2 (as dominant neutral constituent) on associated total absorption at 8, 16 and 24 MHz. H and UH denote heated and unheated ionospheric conditions, respectively. The OX subscript corresponds to difference in O- and X-mode absorptions. The absorption calculation associated with increased N_2 and N_e by a factor of 2 is presented.

Typical variation of HF absorption profile versus altitude is studied in Figure 3. The electron density profile is assumed to increase linearly from 60 to 90 km (10^7 to 10^{10} m^{-3}). Constant electron density of 10^{10} m^{-3} is considered for altitude range of 90 to 110 km. The region is zoomed in in comparison with previous figures to show the detailed variation of absorption profiles. Hf frequencies of 3, 8, 14, 21, and 28 MHz are used. A typical electron temperature profile of Figure 3b is used. A substantial reduction in maximum absorption amplitude is seen as the frequency decreased from 8 MHz to 3 MHz. The figures show that the maximum absorption is mainly limited to the altitude range of 75 to 95 km. This altitude range increases for the X-mode. Results associated with X-mode reveal larger variation concerning higher frequencies used in this study. Another interesting change observed in Figures 3d and e is the negative effect of HF pump heating (increased T_e/T_i) on absorption profile at low frequencies and altitudes below 75 km. A more detailed study of the results is provided in Table 3 based on the measurable parameters in the actual experiment.

Table 3 represents the total absorption of O-mode and X-mode in the unheated and heated D-region as well as the total phase variation of the propagating signal at 3, 8, 16, 24, and 28 MHz. The absorption amplitude in dB per kilometer (dB km^{-1}) is shown for different altitudes from 60 to 110 km. According to this Figure, the maximum absorption is 0.23, 0.03, 0.0086, and 0.004 dB km^{-1}, as the frequency changes from 3 to 28 MHz. These values for the X-mode is 12, 0.06, 0.0122, 0.0036, and 0.004 dB km^{-1} for transmission frequencies of 3, 8, 16, 24 (and 28) MHz, respectively. The close comparison of the absorption value for the O-mode and X-mode shows that this technique along with 5-implemented frequencies has a unique signature and can be used to determine the mesospheric parameters based on the amount of absorption. Considering the predictable scale of absorption at the selected frequency bands, the received signal on the ground can also be corrected to the original amplitude. The corrected signal then can be used for other applications such as deriving the scintillation parameters to determine ionospheric irregularities. This is the subject of another paper that explains the applications of the proposed HF beacon in studying gravity waves and ionospheric tomography.

3.1 Neutral Density

Another parameter that has been investigated in this study is the effect of neutral density variation on the absorption at different transmission frequencies, in the artificially modified condition by high-power radio waves as well as natural D-region condition, and O- and X-mode signals. The electron-neutral collision frequency is directly related to the neutral densities as shown in the following expression (Schunk and Nagy, 1978)

$$\nu_{en} = 2.33\times10^{-17}N_2(1-1.21e^{-4}T_e)T_e+1.82\times10^{-16}O_2(1+3.6e^{-2}\sqrt{T_e})\sqrt{T_e}+8.9\times10^{-17}O(1+5.7e^{-4}T_e)\sqrt{T_e} \tag{14}$$

Figure 4 represents the neutral densities of N_2, O_2, and O atoms obtained from the MSIS model. The variation of absorption amplitude per kilometer for transmission frequencies of 16 MHz and 28 MHz as a result of neutral density increase by a factor of 2 is investigated. Figures show the variation of O- (blue lines) and X-mode (black lines) absorption (dB km^{-1}) as the neutral densities of N_2, O_2, and O are increased. According to this figure, a change of O_2 density by a factor of 2 makes a negligible impact on the absorption profile in the heated ionospheric plasma. N_2 increase produces maximum absorption change by a factor of $\sim$1.8 in both O- and X-modes. In unheated ionospheric conditions, O_2 and N_2 increase by a factor of 2 2 produce a notable change in the absorption profile versus altitude. Both frequencies show a similar trend for heated and unheated ionospheric plasma. According to Figure 4 in the unheated condition and transmission frequency of 16 MHz, the maximum absorption amplitude changes from 0.0087 in the natural condition to 0.0105 and 0.0157 dB km^{-1}, for the enhanced O_2 and N_2, respectively. It should be noted that an increase of O density by a factor of 2 does not affect the absorption amplitude with respect to the natural condition. A similar trend with a smaller variation has been observed for the X-mode at 16 MHz. The main feature observed in the results presented in Figure 4 is that the unheated ionospheric condition shows a distinct behavior for increased background N_2, O_2, and O densities. Such a distinct effect is essential for the concept proposed in the following section. Moreover, while elevated electron temperature will add additional information regarding the absorption change at different frequencies it alone can't provide the measurement of atmospheric constituents as promised in this paper. As mentioned in the text, more experimental observations are required to determine the best cooling model for estimation of HF absorption in the modified ionospheric conditions using high-power HF radio-waves. Then, the absorption models and proposed technique in section 5 can be implemented for possible D- and E-region measurements.

It should be noted that the technique introduced in this paper uses total absorption at each frequency and for different modes produced over the altitude range of 60 to 130 km. Therefore, a combination of experiments in both natural and heated ionospheric conditions could help to resolve unexpected atmospheric conditions.

3.2 Electron Density

The previous work by Senior et al. (2010) has investigated the effect of the electron density variation on the absorption parameter. The results have shown that maximum error produced in the absorption value as the electron density changes by a factor of 2 is of the order of 30 percent. Therefore, implementing more frequencies can eliminate such errors. Using other measurement sources for electron density such as Total Electron Content (TEC) with ground GPS receivers or Ionosonde observations of electron density profile would result in a detailed calculation of D-region absorption. On the other hand, eliminating the absorption effects in order to study the induced by plasma irregularities on the signal path as well as associated ionospheric phenomena such as scintillation, gravity waves, plasma instabilities are the advantages of the proposed mission with multi-frequency transmission and reception in the HF band. The phase data and Faraday rotation measurements at 5 frequencies could also lead to a more accurate measurement of TEC and make this approach self-consistent with other techniques discussed above.

The variation of absorption over the entire D-region for the O-mode in the heated (H) and natural (UH) ionosphere (ΔA_OH-UH), X-mode (ΔA_XH-UH), as well as differential absorption of O- and X-modes in the heated ionosphere (ΔA_{OX} H) and unheated (UH) ionospheric conditions (ΔA_{OX} UH) for transmission frequencies of 8, 16, and 24 MHz are shown in Table 4. The main purpose of the proposed mission (so-called REEMA) is to measure the total absorption of the signal and also derive the ionospheric parameters. Extracting the neutral densities such as N_2, electron density, and temperature variation during radio wave heating of the ionosphere.

4 Machine Learning

The possibility of HF absorption observations on the ground using simultaneous multi-frequency observation to determine background parameters in the D- and E-regions are explored in this section. Specifically, total absorption of radio signal passing through lower ionospheric region along with the model simulation results of total absorption are incorporated to determine middle atmosphere temperature and composition. This includes both constituent and temperature observations that have a wide application in studying the physics and chemistry of the middle and upper atmosphere. A machine learning is developed to achieve this goal. A year of data of neutral atmosphere from MSIS model and electron density from IRI model are used to educate the model. The selected data from 2019 are imported for the detailed absorption calculations using the model described in sections 2 and 3. Then two days from 2018 and 2020 are selected to validate the model performance and accuracy.

The results for two days in a year before and after the trained database is used. Figures 6 and 7 show the machine learning results associated with 2018-2-5 and 2020-2-2, respectively. The diagram shown in Figure 5a represents the main idea of data assimilation presented in this paper. A simplified version of the model has been developed to examine the main idea of the paper. A machine learning approach is adopted to evaluate the performance of the introduced technique to determine the atmospheric constituents, electron density, and neutral temperature in the mesosphere. To achieve this goal, the algorithm is implemented by a collection of neutral density data through the MSIS model as well as electron density profile in the altitude range of 60 to 130 km. The data is collected every other day with hourly time resolution. A flow chart describing the ML approach is shown in Figure 5b. The total HF absorption at 5 frequencies (4, 8, 12, 16, and 20 MHz) are used to run the ML model and estimate the D and E-region constituents including N_2, O, O_2, as well as T and N_e. It should be noted that only total absorption data are incorporated in the ML model and the phase data due to possible uncertainty in the actual observation is excluded.

The machine learning (ML) procedure has been exploited to find the unknown constituents of D-layer according to the direct measurements of signal absorption for multiple frequencies in the HF band (4, 8, 12, 16, 20, and 24 MHz) and two modes (O and X). The procedure flowchart is illustrated in Figure 5b. It can be seen that for learning process, the data of T_e, N_e and N_2, O_2, and O were captured from IRI and MSIS models (TeL, NeL, nN2L, nOL, nO2L), respectively for altitude of 60-130 Km with 0.1 km resolution. The time resolution of them was every hour with the cardiac cycle for some days in every month of the year 2019. After capturing these learning data, their proportional absorptions in O and X-mode for multiple frequencies (f) in HF band (AL (TeL, NeL, nN2L, nOL, nO2L, mode, f)) were calculated according to the general form of Appleton-Hartree dispersion formula. In these calculations, the effect of the earth's magnetic field in all sampling altitudes and the collision frequency averaged over the electron velocity distribution function were considered. Thus, it can be said that the collision frequency has been defined as an effective electron-neutral collision frequency as a function of the contributions for several different neutral species (Schunk and Nagy, 2009). To simulate the measurement setup, data capturing from MSIS and IRI sites have been done for a random time and date of a year (TeR, NeR, nN2R, nOR, nO2R), then the same absorption calculation process as the learning step was handled for them AR(TeR, NeR, nN2R, nOR, nO2R, mode, f). The cost function (CF) was defined based on the absolute value of differences between the absorption of randomly sampled data and one of the learning data for multiple frequencies and two modes ($CF = |AL - AR|$). Hereafter, the CFs were processed in two distinct ways according to modes. In each of them, the best (minimum) CF was found among the cost functions of multiple frequencies. After that, the proportional constituents' profiles according to the best CF were assigned for the estimated one. In the next step, to enhance the best CF, i.e. to minimize much more, partial optimization based on Te Ne variations of assigned profiles has been done. Ultimately, the final estimated constituents' profiles were obtained by averaging two optimized constituents' profiles found at O/X mode process state.

The results for two days in a year before and after the trained database is used. The machine learning results are obtained in unperturbed ionospheric conditions. The days and hours selected to examine the ML results are out of the dates used to learn the model. As can be seen the error in the prediction of neutral densities including N_2, O, and O_2 is negligible. The neutral temperature profile shows agreement with the data. The altitude profile of estimated electron density matches well the original data used to

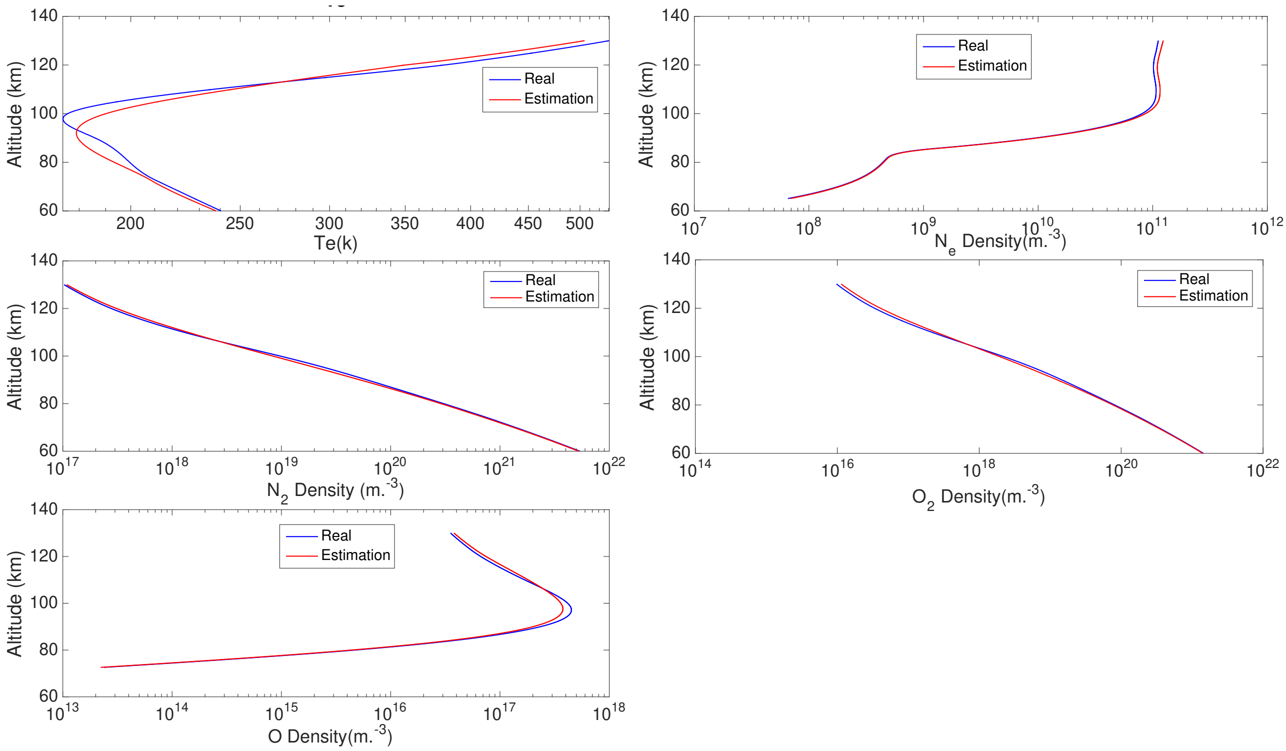

Figure 5. Machine learning (ML) results for 2018-2-5. The red line denoted the estimated results from ML model and blue line are the data obtained for the same date and time associated with the simulations.

calculate the respected total HF absorption at the selected frequencies. It should be noted that implementing the HF modulation in the on and off period will result in higher accuracy.

5 Global mapping of HF absorption in the northern hemisphere

To implement the technique described in section 4, a global map of HF absorption needs to be considered. In fact, distribution of ground HF receiver to monitor multi frequency total HF absorption simultaneously requires to probe the latitude range with high sensibility. Therefore, the global map of HF absorption at two frequencies are examined in this section. Diurnal and monthly variation of total HF absorption in the northern hemisphere are presented. To calculate HF absorption map in the northern hemisphere, a fixed longitude of 51.3347° E is used. Neutral densities are obtained from MSIS model for entire year. The data collected in latitude range 0 to 90 degrees with 1 degree resolution. The corresponding electron density is obtained using IRI model. The empirical data are selected for the year of 2019. The total absorption in the altitude range of 70 to 140 km is calculated. The results for global map of HF absorption for O-mode propagation at 4 MHz are shown in Figure 8, respectively. The results are obtained in natural ionospheric condition without HF radio wave heating. According to Figure 8, total absorption reaches 15 dB in the altitude range of interest. The global map in entire year shows a similar pattern with a maximum absorption extended in the latitude range of 0 to 20 degrees. There is a small extension of high absorption rate to higher latitudes in the summer. As a comparison, the results associated with 16 MHz is presented in Figure 9. While the global pattern of HF absorption in entire year remains similar to 4 MHz, the maximum absorption is reduced to 0.6 dB. The absorption for the X-mode is much

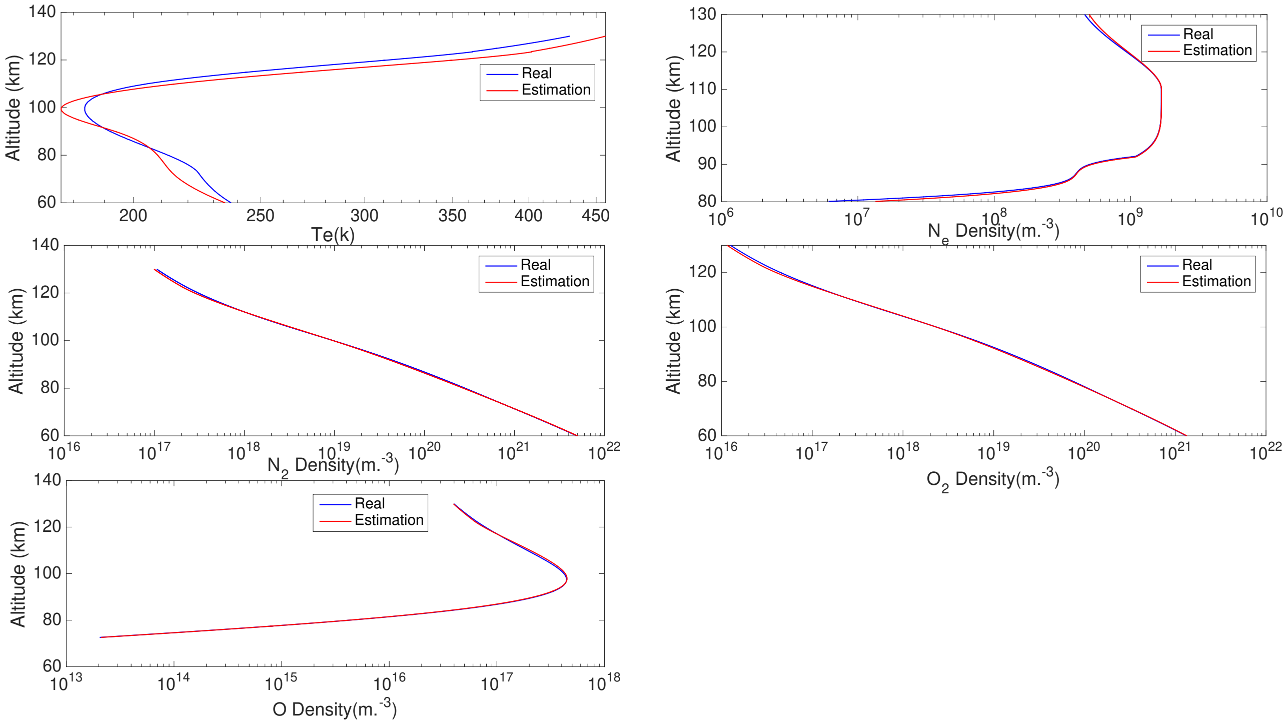

Figure 6. Machine learning (ML) results for 2020-2-2. The red line denoted the estimated results from ML model and blue line are the data obtained for the same date and time associated with the simulations.

higher in comparison with the O-mode (not shown in this paper). The results presented in the paper can be implemented to improve OTHR observations as well as oblique ionosonde sounding. Moreover, the technique described in section 4 appears to be practical and sensitive to high latitudes.

6 Summary and conclusions

In summary, the concept of developing a multi-frequency HF radio sounding technique for detailed measurement of the D-region absorption is investigated in this paper for the first time. The detailed calculations of absorption amplitude (dB km^{-1}) and total phase variation in the natural D-region condition, as well as an artificially modified condition by a high-power radio wave, are considered. The HF absorption profiles and total HF absorption are calculated using the Garrett and Appleton–Hartree formula of refractive index. It has been shown that there is a small difference in estimated HF absorption between the two models, especially in unheated ionospheric conditions. The effect of three cooling formulation associated with N_2 and O_2 vibrational and rotational excitation was found to be negligible in natural ionospheric condition. Performing such experiments in heated and unheated ionospheric plasma could be used to calibrate the instrument and to use the best cooling model and refractive index for the artificially modulated lower ionosphere.

The two O-mode and X-mode transmissions along with transmission frequencies of 2, 8, 16, 24, and 28 MHz associated with the proposed REEIMA HF beacon (Radio Explorer for Earth, Ionosphere, Mesosphere, and Atmosphere) are used to determine the absolute D-region absorption along with the possibility of estimating D-region param-

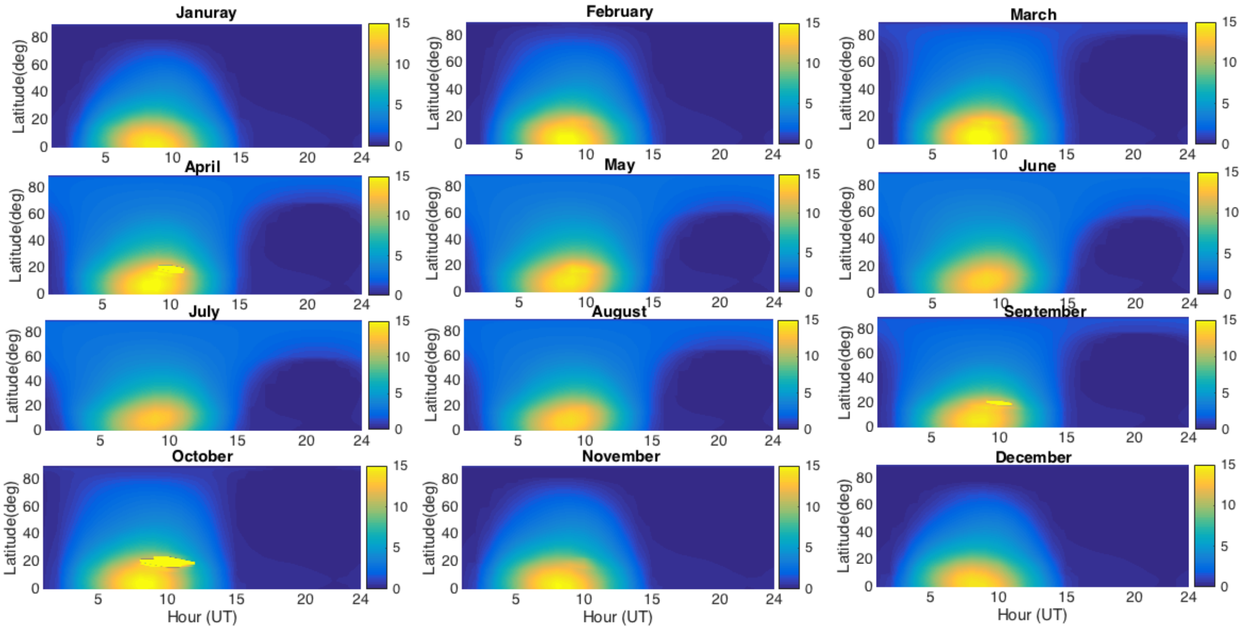

Figure 7. The global map of HF absorption in the northern hemisphere associated with the empirical data obtained using MSIS and IRI model for 2019. The HF transmission with O-mode polarization at 4 MHz is used. A fixed longitude of 51.3347° E is used in the calculations. The color bar shows the total absorption in dB.

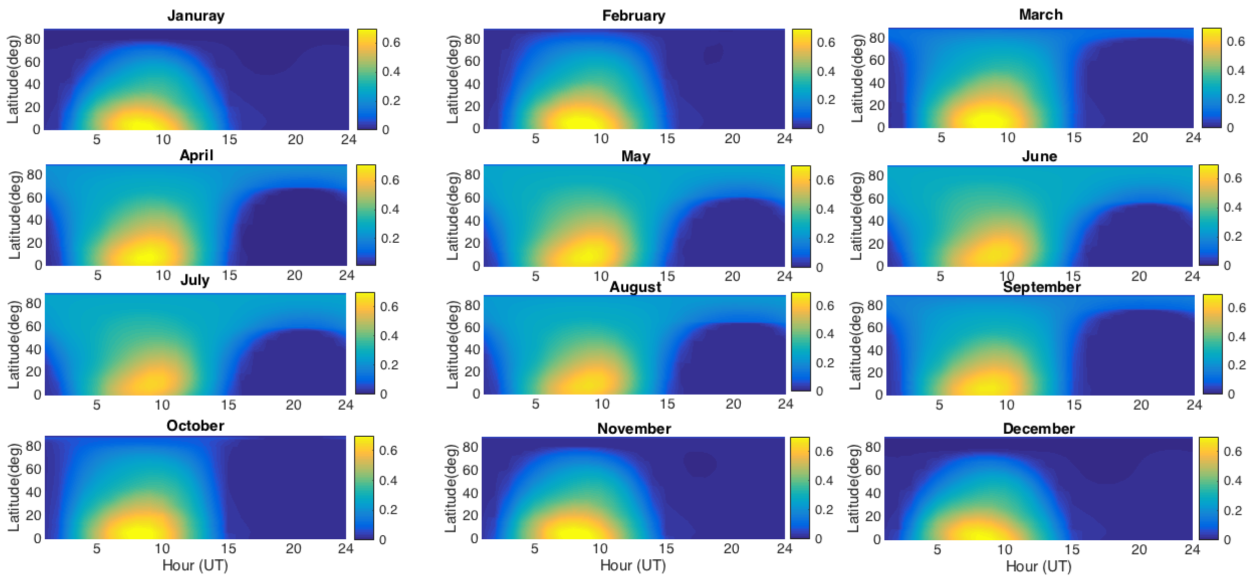

Figure 8. Similar to Figure 7 for 16 MHz.

eters such as neutral densities as well as removing the absorption from the transmitted signal. It has been shown that the variation of each background neutral density including N_2, O_2, and O produces a distinct effect on the absorption value of O- and X-mode as well as different transmission frequencies. A machine learning technique is developed based on the model simulation results using the empirical data from the MSIS and IRI models for 2019. The accuracy of model appears to be encouraging for the estimation of the background temperature and neutral density profiles. Moreover, Therefore, the proposed technique can eliminate the effect of electron density variation and the possible error in OTHR measurement by using temporal evolution of HF absorption. It should be noted that previous studies have shown that riometers may overestimate the absorption by a factor of 2 in the modified D-region conditions by high-power radio waves despite changes in electron density and heater parameters.

Moreover, the global map of HF absorption in the northern hemisphere associated with two transmission frequencies of 4 and 16 MHz are presented. It has been shown that diurnal and seasonal variation of global HF absorption is pronounced enough for such a technique to be implemented globally with a distributed network of HF receivers on the ground. The mission can be implemented to improve OTHR and SuperDARN observations in the both hemispheres.

Acknowledgments

This work is supported by ISEF (Iran Saramadan Elmi Federation). The model used in this paper is available through https://github.com/alirezam1983/JGR-SPACE-PHYSICS.git.

References

Bernhardt, P. A., Huba, J. D., Chaturvedi, P. K., Fulford, J. A., Forsyth, P. A., Anderson, D. N., and Zalesak, S. T.: Analysis of rocket beacon transmissions for computerized reconstruction of ionospheric densities, Radio Sci., 28(4), 613– 627, doi:10.1029/93RS00383, 1993.

Bernhardt, P. A and Huba, J. D.: Reconstruction of non-stationary plasma irregularities using ionospheric tomography, Cospar Colloquia Series: Low-Latitude Ionospheric Physics, Taipei, November, 1993.

Bernhardt, P. A., McCoy, R. P., Dymond, K. F., Picone, J. M., Meier, R. R., Kamalabadi, F., Cotton, D. M., Chakrabarti, S., Cook, T. A., Vickers, J. S., Stephan, A. W., Kersely, L., Pryse, S. E., Walker, I. K., Mitchell, C. N., Straus, P. R., Na, H., Biswas, C., Bust, G. S., Kronschnabl, G. R., and Raymund, T. D.: Two dimensional mapping of the plasma density in the upper atmosphere with computerized ionospheric tomography (CIT), Phys. Plas., 5, 2010–2021, 1998.

Bernhardt, P. A., Huba, J. D., Selcher, C. A., Dymond, K. F., Carruthers, C. R., Bust, G., Rocken, C., and Beach, T. L.: New Systems for Space Based Monitoring of Ionospheric Irregularities and Radio Wave Scintillations, Space Weather, Geophysical Monograph 125, 431–440, AGU, 2001.

Bernhardt, P. A., Selcher, C. A., Siefring, C., Wilkens, M., Compton, C., Bust, G., Yamamoto, M., Fukao, S., Ono, T., Wakabayashi, M., and Mori, H.: Radio tomographic imaging of sporadic E-layers during SEEK2, Ann. Geophys., 23, 2357–2368, 2005.

Bernhardt, P. A., and C. L. Siefring: New satellite-based systems for ionospheric tomography and scintillation region imaging, Radio Sci., 41, RS5S23, doi:10.1029/ 2005RS003360, 2006.

Campbell, L., M. J. Brunger, D. C. Cartwright, and P. J. O. Teubner: Production of vibrationally excited N2 by electron impact, Planet. Space Sci., 52, 815 – 822, 2004.

Caton, R., McNeil, W., Groves, K., Basu, S.: GPS proxy model for real-time UHF satellite communications scintillation maps from the Scintillation Network Decision Aid (SCINDA). Radio Science - RADIO SCI. 39. 10.1029/2002RS002821, 2004.

de La Beaujardiére, O.: C/NOFS: a mission to forecast scintillations. Journal of Atmospheric and Solar-Terrestrial Physics, 66(17), 1573– 1591. https://doi.org/10.1016/j.jastp.2004.07.030, 2004.

Evans, J. V.: Satellite beacon contributions to studies of structure of the ionosphere, Rev. Geophys., 15, 325–350, 1977.

Friedman, H.: Rocket observations of the ionosphere, Proc. Inst. Radio Eng., 46, 272–280, 1959.

Garrett, A. J. M.: Multi species kinetic generalization of the Appleton-Hartree dispersion formula, J. Plasma Phys., 33, 265–284, 1985.

Garrett, A. J. M.: Kinetic theory of cross modulation in a weakly ionized plasma, J. Plasma Phys., 46, 365–390, 1991.

Groves, Keith, Basu, S., Weber, E.J., Smitham, M., Kuenzler, H., Valladares, Cesar, Sheehan, R., Mackenzie, Emma, Secan, James, Ning, P., McNeill, W.J., Moonan, D.W., Kendra, M.J.: Equatorial scintillation and systems support. Radio Science. 32. 2047-2064, 1997.

Havnes, O. (2004), Polar Mesospheric Summer Echoes (PMSE) overshoot effect due to cycling of artificial electron heating, J. Geophys. Res., 109, A02309, doi:10.1029/2003JA010159.

Jackson, J. E.: Measurements in the E layer with the Navy Viking rocket, J. Geophys. Res., 59, 377–390, 1954.

Jones, D. B., L. Campbell, M. J. Bottema, and M.J. Brunger: New electron-energy transfer rates for vibrational excitation of O_2, New J. Phys. 5 114. https://doi.org/10.1088/1367-2630/5/1/114, 2003.

Maeda, K. I.: Radio propagation effects used on rockets in probing the ionosphere, J. Atm. Solar-Terr. Phys., 32, 647, 1970.

Mahmoudian, A., Kosch, M. J., Vierinen, J., and Rietveld, M. T. (2020). A new technique for investigating dust charging in the PMSE source region. Geophysical Research Letters, 47, e2020GL089639. https://doi.org/10.1029/2020GL089639

Pavlov, A.V.: New electron energy transfer rates for vibrational excitation of N2, Ann. Geophys., 16, 176-182, 1998a.

Pavlov, A.V.: The role of vibrationally excited oxygen and nitrogen in the ionosphere during the undisturbed and geomagnetic storm period of 6-12 April 1990, Ann. Geophys., 16, 589-601, 1998b.

Pavlov, A.V.: New electron energy transfer and cooling rates by excitation of 02, Ann. Geophys., 16, 1007-1013, 1998c

Scales, W.: Electron temperature eects on small-scale plasma irregularities associated with charged dust in the Earths mesosphere. IEEE Transactions on Plasma Science, 32, 724, 2004.

Scales, W. A., and Mahmoudian, A.: Charged dust phenomena in the near Earth space environment. Reports on Progress in Physics, 79(10), 106802. https://doi.org/10.1088/0034-4885/79/10/106802, 2016.

Seliga, T. A.: Analysis and results of low-frequency CW Rocket Propagation Experiments in the D region, J. Geophys. Res., 73(21), 6783–6794, doi: 10.1029/JA073i021p06783, 1968.

Senior, A., M. T. Rietveld, M. J. Kosch, and W. Singer: Diagnosing radio plasma heating in the polar summer mesosphere using cross modulation: Theory and observations, J. Geophys. Res., 115, A09318, doi:10.1029/2010JA015379, 2010.

Senior, A., M. T. Rietveld, F. Honary, W. Singer, and M. J. Kosch: Measurements and modeling of cosmic noise absorption changes due to radio heating of the D region ionosphere, J. Geophys. Res., 116, A04310, doi:10.1029/2010JA016189, 2011.

Schunk, R., A. Nagy: Ionospheres: Physics, Plasma Physics, and Chemistry 2nd Edition, Cambridge University Press, 2009.

Schunk, R., A. Nagy: Ionospheres: Physics, Plasma Physics, and Chemistry, Cambridge University Press, 1978.

Smith, L. G. and Gilchrest, B. E.: Rocket Observations of electron density in the nighttime E-region using Faraday-rotation, Radio Sci., 19, 913–924, 1984.